Transactions on Materials, Biotechnology and Life Sciences
ISSN: 2960-1932, eISSN: 2960-2319 | Volume 4
NSCBM 2024

The Application of Pd-Based Nanomaterials for Methanol Oxidation and Oxygen Reduction Reaction in The Direct Methanol Fuel Cells

Runhan Zhai *

Shanghai Guanghua Cambridge International School, Shanghai, China

* Corresponding Author Email: zhailei@cscec.com

Abstract. Direct methanol fuel cells (DMFC) are considered as a sustainable and environment-benign energy source which provide electrical energy from chemical energy with less pollution, higher efficiency, and noiseless operation. In this review, the application of the Pd-based nanomaterials for the oxygen reduction reaction(ORR) that is carried out on the cathode and the methanol oxidation reaction(MOR)that is carried out on the anode are discussed in the direct methanol fuel cells. At first, the mechanisms of ORR and MOR will be described. Then, the bimetallic and multi-metallic nanomaterials including Au/C-Pd/C, Pd_3Sn/CNTs NHs, and Pd_3Ag_1/meso-CeO_2 will be summarized focusing on stability, the catalytic activity and performance for ORR. Furthermore, supports like reduced graphene oxide (rGO) with modified POM, carbide-derived carbon (CDC), and nitrogen-doped graphene quantum dots (NGQD) that Pd nanoparticles (NPs) are deposited on will influence the activity of the catalysts for ORR. The study for the use of Pd/TiO_2 decorated carbon fibers for methanol oxidation will also be discussed and the effects of different TiO_2 mass fractions on conductivity, EASA value, and electrochemical activity will be summarized.

Keywords: Palladium, nanomaterial, methanol oxidation, oxygen reduction, fuel cell.

1. Introduction

Recently, energy sources like fossil fuels have polluted the environment, thus it is important to find sustainable and environment-benign energy sources [1]. Direct methanol fuel cells (DMFC) are considered as an ideal and good device which provide electrical energy from chemical energy with less pollution, higher efficiency, and noiseless operation [2]. In both ORR and MOR, the catalysts play an important role. Platinum-based catalysts used to be the best and most effective catalysts for the ORR and methanol oxidation reaction, but they have many disadvantages including short storage, expensive Pt metal, and high cost for developing Pt-based catalysts. Therefore, the Pt metal is replaced by Pd [2]. As palladium metal is also expensive, Pd-based nanomaterials will act as the major catalysts in the DMFCs [3]. In order to enhance catalytic activity of Pd-based nanomaterial, Pd-based bimetallic and multi-metallic nanomaterials are used. The effects of amounts and size of Pd-based catalysts on both reactions will be discussed. The mass activity, specific activity and kinetic current energy of the Pd-based catalysts will also be mentioned. Moreover, the properties and structure of the supports including the conductivity, chemical stability, electron transport, microspores and mesopores will be focused on in this review. The interaction between the metal loading and supports also enhances electro-catalytic activity. Besides, how the durability and the stability of the Pd-based catalysts are improved will also be discussed in this review.

2. Mechanisms

In the DMFC, the the MOR occurs at the anode and ORR occurs at the cathode. The ORR will be carried out in both direct and series ways (**Figure 1)**. In an acidic medium, the oxygen will gain 4 electrons and form two water molecules. This pathway is better than the series pathway because H_2O_2 which is harmful will not form. In an alkaline medium, the oxygen will gain 4 electrons and form 4 hydroxide ions in the direct pathway, and Pd–based nanocatalyst shows a high catalytic activity [3].

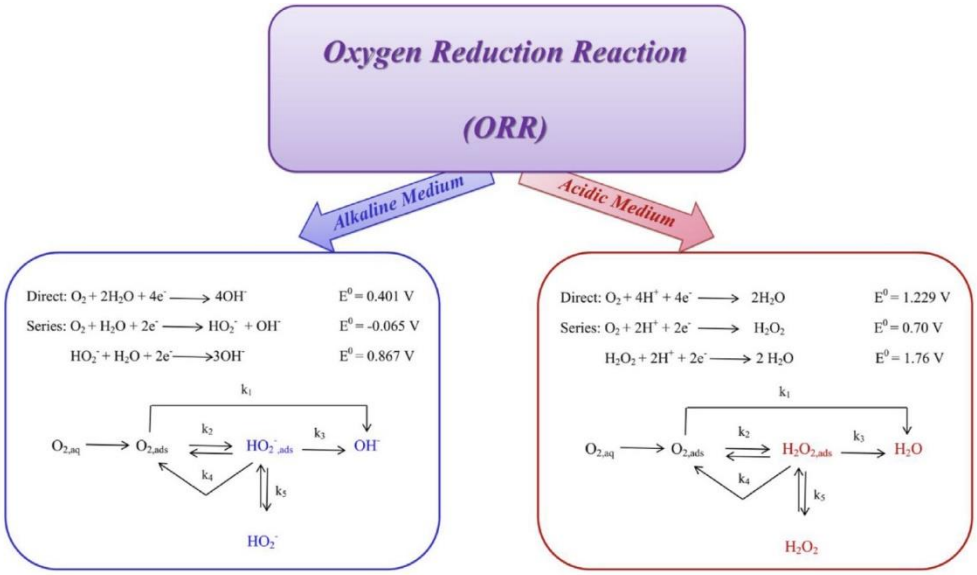

Figure 1. ORR in basic and acidic medium [3].

In the acidic medium, carbon dioxide is formed from methanol oxidization at the anode while carbonate ions is produced in the alkaline medium (**Figure 2**.) [4].

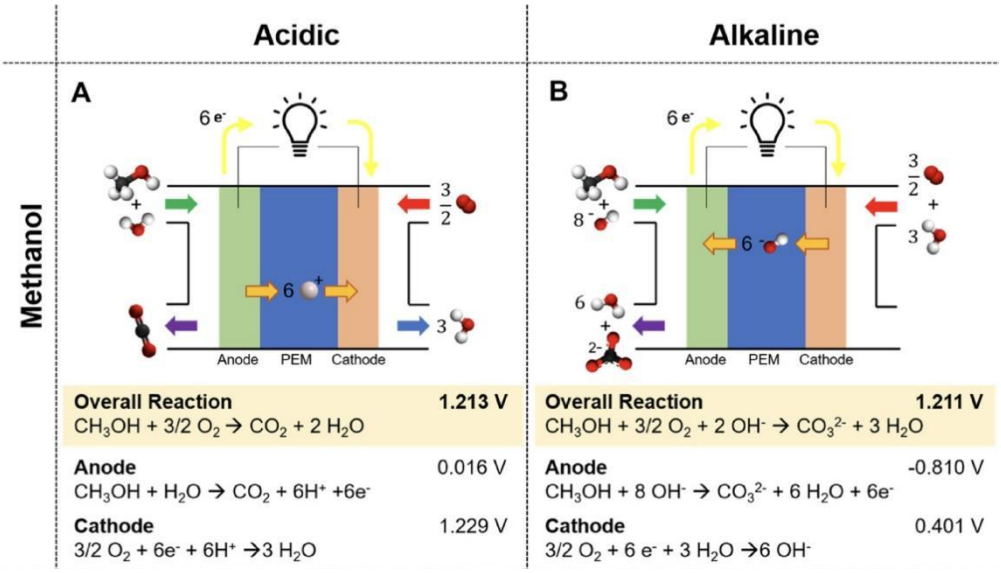

Figure 2. The MOR in acidic and basic medium [4].

3. The application of Pd-based bimetallic, and multi-metallic nanomaterials for ORR

3.1. Bimetallic Au–Pd systems in aerobic oxidation

For the monometallic Pd/C catalyst, the carbon support provides a high conductivity for electron transport with the oxidative dehydrogenation (ODH) of 5-hydroxymethylfurfural (HMF) (**Figure 1.**). As shown in the TEM experiment (**Figure 2.**), the Pd/C exhibits a high catalytic performance with a narrow particle size distribution and small average particle size [5].

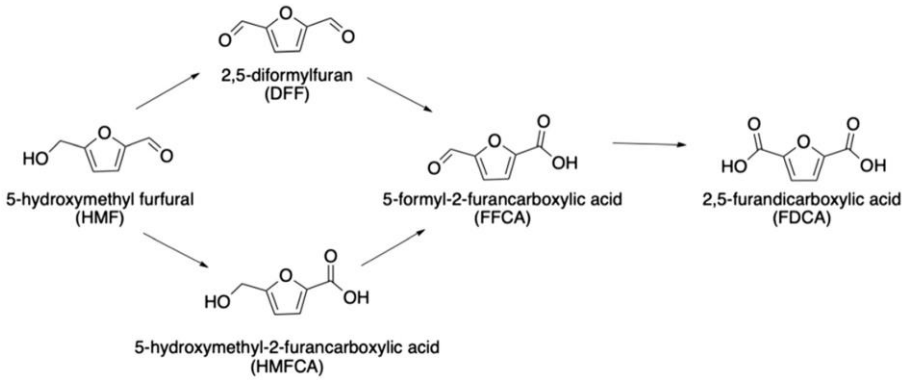

Figure 3. The oxidative dehydrogenation of HMF. [5]

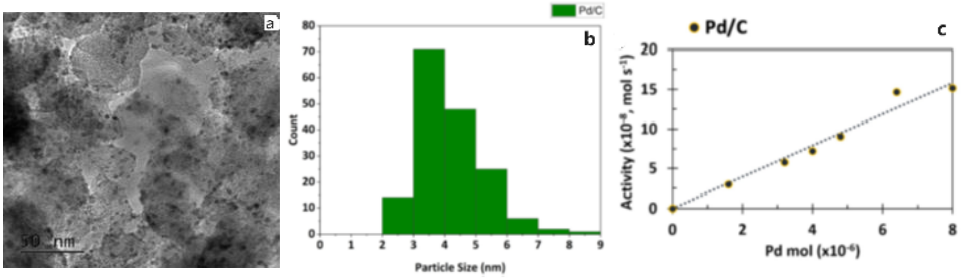

Figure 4. Experimental data for 1 wt% Pd/C. (a) TEM image of 1 wt% Pd/C. (b)associated particle size distribution of 1 wt% Pd/C. (c)Pd activity as Pd content increases.[5]

For bimetallic Au–Pd systems, the rate of ODH is intrinsically associated with the rate of ORR (Figure 5.). The resulting acceleration of the coupling rate is evaluated by kinetic analysis. The effect of the molar ratio of Pd / Au is studied for a mixture of carbon-supported catalysts via changing the mass of each 1 wt% catalyst (Figure 6.). Significantly, higher activity of the bimetallic system is always observed than the sum of the monometallic analogues. With the coupling between ODH and ORR considered, where the highest bimetallic and monometallic activity will be observed could be predicted via kinetic analysis. Further evidence and insight of cooperative redox enhancement (CORE) effects of bimetallic catalytic systems could be provided by the accuracy of the model. [5]

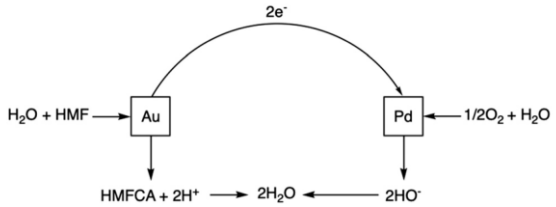

Figure 5. The proposed CORE system of ODH on Au sites and ORR on Pd sites.

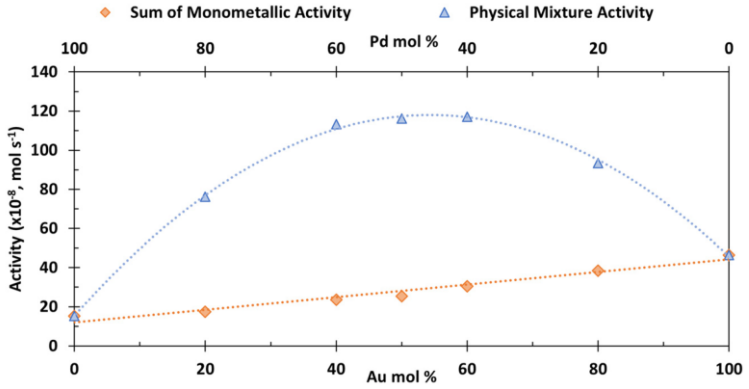

Figure 6. Comparation of Physical mixture activities and the sum of monometallic activities at various molar ratios of Au and Pd.

3.2. Pd_3Sn/CNTs NHs

The PdxSny/CNTs NHs is the general formula of the multi-metallic nanocrystal on carbon nanotubes. A group of PdxSny nanocrystals including Pd_3Sn, Pd_2Sn, Pd_3Sn_2, and PdSn have been distributed and anchored on the carbon nanotubes through a hydrolytic system with a thermolysis method in one pot. Among these nanocrystals, the Pd_3Sn nanocrystal on the CNTs shows the best ORR ability and capability. The Sn with a high valence can be easily oxidized into SnOx, which has a high affinity with oxygen and the electron will be transferred from Sn to Pd. Therefore, the existence of Sn can somehow inhibit the oxidation of Pd. Through TEM image, Pd3Sn nanocrystals are found in small size and arranged into a network, surrounding the surface of the whole CNTs, forming the Pd_3Sn/CNTs nanohybrids and promoting the electron conduction, electrolyte infiltration, stability and catalytic activity [6].

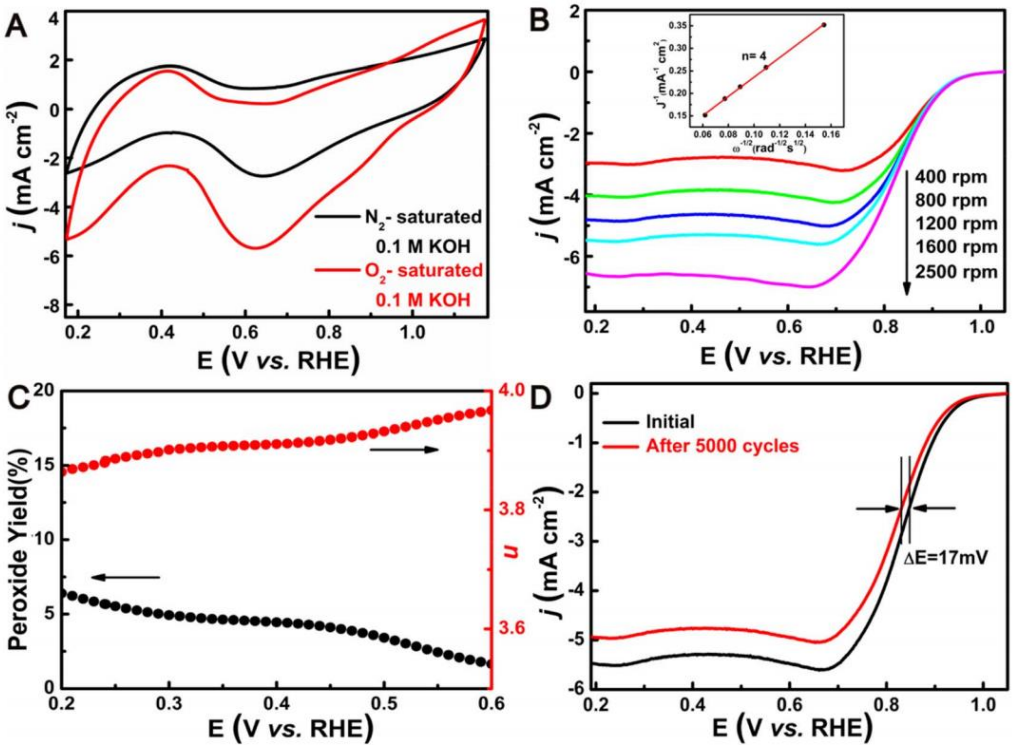

Figure 7. Activity of Pd_3Sn/CNTs NHs for ORR (A). The CVs. (B). ORR polarization plots. (C). The number of transferred electrons (n) (red) and the yield of peroxide species (black). (D). The durability test [6].

In **Figure 7A**, the small peak around 0.83V demonstrated the activity of Pd_3Sn/CNTs NHs for ORR. Compared with pure CNT and pure Pd_3Sn NCs, the Pd_3Sn/CNTs NHs have higher onset potential, halfwave potential, and current density. **Figure 7B** shows n during ORR is about 4.0, which means that $4e^-$ is accepted by O2 to form OH^- in alkaline conditions and Pd_3Sn/CNTs NHs follow a "$4e^-$" pathway. Meanwhile, **Figure 7C** shows that the percentage yield of the peroxide species (HO_2^-) on Pd_3Sn/CNTs NHs was much lower than pure CNT and pure Pd_3Sn NCs at different potentials, emphasizing the high ORR efficiency. Moreover, in **Figure 7D**, after 5000 CV cycles, Pd_3Sn/CNTs NHs has a smaller negatively shift than that of Pt/C catalyst, demonstrating the advanced ORR ability of Pd_3Sn/CNTs NHs [6].

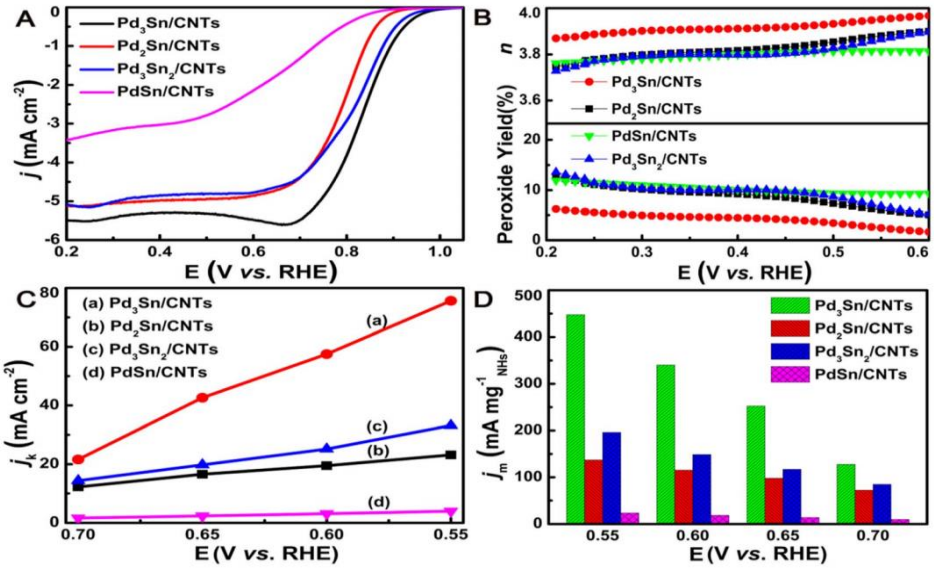

Figure 8. Comparison between the Pd_3Sn/CNTs, Pd_2Sn/CNTs, Pd_3Sn_2/CNTs and PdSn/CNTs. (A) ORR polarization plots at 1600 rpm. (B) The yield of peroxide species and n. (C) Kinetic current density (Jk) VS potential plots. (D) Mass-specific activities [6].

In comparison with Pd_2Sn/CNTs, Pd_3Sn_2/CNTs and PdSn/CNTs, Pd_3Sn/CNTs own the lowest percentage yield of peroxide, the highest value of n (about 4), the greatest kinetic current density and mass activity (Figure 8.) [6].

3.3. Bimetallic Pd–Ag alloy supported on mesoporous cerium oxide:

The characteristics of the bimetallic Pd-Ag alloy are similar to the bimetallic Pd-Sn alloy. Comparing meso-CeO_2 with PdAg/meso-CeO_2 and Pd_3Ag/meso-CeO_2, with the decoration of Ag or Pd-Ag alloy, the peak potential of ORR moves positively and Pd_3Ag/meso-CeO_2 demonstrate the greatest positive shift of ORR peak potential. Thus, the Pd3Ag1/meso- CeO_2 catalyst shows good electro-catalytic activity. Moreover, Pd_3Ag/meso- CeO_2 has a higher ECSA (electrochemical active surface area) than the Pd1Ag1/meso-CeO_2 and Pd_2Ag/meso- CeO_2. The Pd-Ag alloy (ratio = 3:1) has a good dispersion on the meso- CeO_2 support and thus Pd_3Ag/meso- CeO_2 catalyst are more electrochemical active for ORR. Similar to the Pd3Sn, Pd_3Ag has the highest onset potential (0.970 V) and highest halfway potential (0.86 V). In comparison to meso- CeO_2 and Ag/meso- CeO_2, PdAg/meso- CeO_2, Pd_2Ag/meso- CeO_2 and Pd_3Ag/meso-CeO_2 has higher onset potential and halfway potential, indicating that Pd is significant for the electro-catalytic activity. There is a positive relationship between the half-wave potentials (E1/2) and the electro-catalytic activity. Additionally, in the ORR process all of the Pd–Ag alloy-loaded catalysts carry out four electron pathways. The Pd_3Ag/meso-CeO_2 also shows a specific activity and mass activity (Table 1) [7]

Table 1. Comparison of ORR kinetics for various electrocatalysts [7].

S. no	Electro catalyst	ECSA(m2g-1)	Jd(mA cm-2)	Eo(V vs RHE)	E1/2(V vs RHE)	n	MA(mA mg-1)	SA(mA cm-2)
1	Pt/C	77.01	5.33	0.974	0.811	4.01	125	0.162
2	PdAg/meso-Ceo2	34.66	3.55	0.913	0.795	2.81	63	0.184
3	Pd2Ag/meso-Ceo2	48.46	3.75	0.953	0.780	3.56	92	0.190
4	Pd3Ag/meso-Ceo2	76.09	4.80	0.970	0.860	3.98	157	0.206

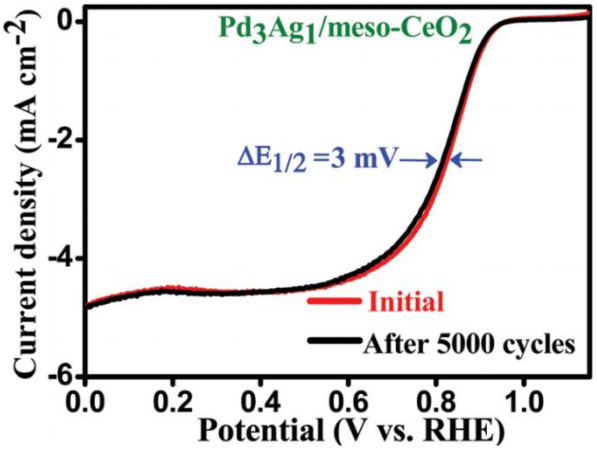

Figure 9. Pd3Ag/meso-CeO2 before and after 5000 cycles at 1600 rpm [7].

Lastly, the durability of the catalysts is also considered and tested. In **Figure 9**, the E1/2 of the Pd_3Ag/meso-CeO_2 only negatively shifts 3mV after 5000 cycles which is much smaller than other catalysts. In the chronoamperometric method, the stability of Pd_3Ag/meso-CeO_2 is tested and this catalyst shows good stability as the loss in current density is not significant and the current reaction also remains at high efficiency (86%) even after a long time [7].

4. Application of Pd-based NPs on different support for ORR

4.1. Polyoxometalate-modified palladium–nickel/reduced graphene oxide alloy catalyst (Pd_8Ni_2/rGO-POM)

When Ni is added to Pd, the alloyed Ni-Pd NPs are formed and the small Ni-Pd are distributed and deposited uniformly on the rGO. The Pd_8Ni_2/rGO is then decorated by POM, forming Pd_8Ni_2/rGO-POM. Compared with Pd_8Ni_2/rGO and Pd/rGO catalysts, Pd_8Ni_2/rGO-POM showed a more positive peak potential and a higher current density, which indicates an important enhancement in the oxygen reduction activity. There are some reasons for Pd_8Ni_2/rGO-POM with a better catalytic activity. First of all, the strong synergism between Pd and Ni will further promote the catalytic activity and ORR performance. Addition of Ni to Pd will make the Pd lattice contract, leading to a lower oxygen-binding strength and d band positions. However, the electron coupling between Ni and Pd will improve the electronic constructions of Pd, achieving a better oxygen reduction performance. Secondly, the rGO as a suitable support, has high chemical stability and notable electron transport properties. rGO is a porous carbon nanomaterial with more space for dispersion of Pd–Ni NPs, enhancing the diffusion and permeation of oxygen with its rich channels. Thirdly, the modification of POM on the Pd_8Ni_2/rGO catalyst will significantly improve the ORR activity because POM could be adsorbed on the surface of Pd-based catalyst to transfer charges as proton acceptors and conductors [8].

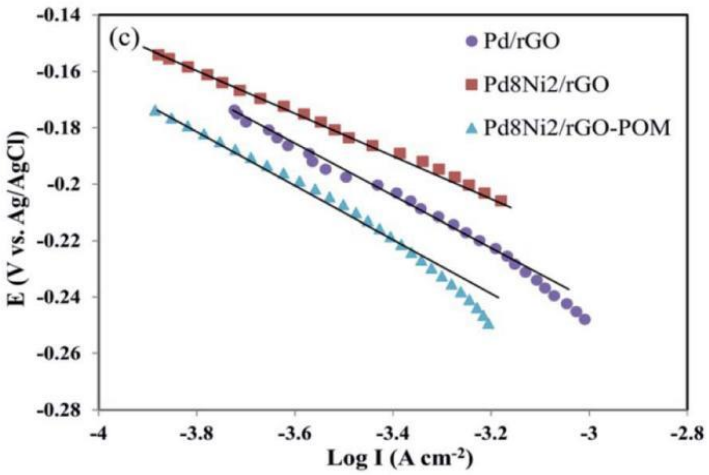

Figure 10. Tafel plots of 3 electro-catalysts [8].

Figure 10 indicates that with the modification of POM on the Pd_8Ni_2/rGO, the gradient of the line gradually becomes more negative, and the slope value decreases, implying that the improvement of ORR kinetics is positively related to the existence of POM [8].

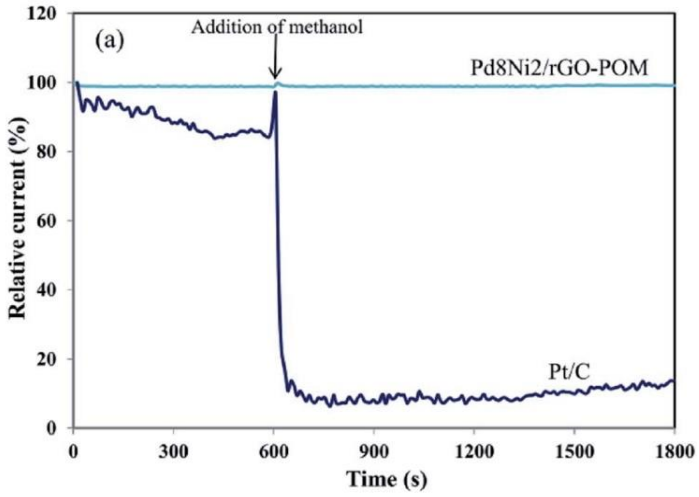

Figure 11. Methanol resistance tests of the commercial and Pt/C Pd_8Ni_2/rGO-POM [8].

The movement of methanol in the fuel cell across the membrane from anode to cathode is called methanol crossover [3]. The methanol crossover will negatively affect the potential equilibrium. In **Figure 11**, the relative current almost remains unchanged after adding methanol into the fuel cells when Pd_8Ni_2/rGO-POM catalyst is used. On the other hand, a sharp decrease in the relative current is observed after adding methanol when using a Pt/C catalyst. These data indicate that the oxidation of methanol will happen when a Pt/C catalyst is used, and the relative current will not recover. However, the relative current will recover after the methanol oxidation by using the Pd_8Ni_2/rGO-POM catalyst. Therefore, the Pd_8Ni_2/rGO-POM catalyst shows desired selectivity towards ORR and resistance to methanol crossover. Thus, Pd_8Ni_2/rGO-POM nanocatalyst become a popular and effective cathodic electrode in DMFC. Moreover, the improved and long-term durability of Pd_8Ni_2/rGO-POM for ORR is due to the consistent distribution of Ni-Pd alloyed NPs on rGO support and the modification of POM [8].

4.2. Pd NPs Supported on Carbide-Derived Carbon

In the preparation of Pd NPs Supported on Carbide-Derived Carbon in one pot, two different methods are used and one of the methods involves the doping with nitrogen and three different carbide-derived carbon supports are used which are CDC1, CDC2 and CDC3 [9].

Table 2. Physical parameters of CDCx/Pd catalysts [9].

Catalyst	Particle size(nm)	Pd LVol-FWHM (nm)	Lattice parameter(Å)	Pd(wt%)
CDC1/Pd_Cit	2.1±0.5	9.80±0.26/1.21±0.01	3.393/3.896	15.0
CDC2/Pd_Cit	2.2±0.5	5.57±0.89/0.60±0.01	3.898	25.5
CDC3/Pd_Cit	1.8±0.4	2.14±0.08/0.50±0.01	3.897	22.6
CDC2/Pd_EG	2.8±0.7	2.09±1.31	3.903	14.8
CDC3/Pd_EG	3.5±1.4	2.18±0.03/7.00±1.45*	3.893/5.1147*	16.8

*Pd_4S.

In **Table 2**, the data shows that the particle size of catalysts increases from CDC1/Pd to CDC3/Pd whether with the citrate ions or ethylene glycol (EG) as the reductant for the catalyst synthesis. However, the particle size of the catalyst is larger when EG is used. [9]

Table 3. Kinetic analysis of the Pd-based catalysts for ORR [9].

Catalyst	ESA(cm^2)	$E_{1/2}$(V)	Tafel slope(mV)*	SA at 0.9V (mA cm^{-2})	MA at 0.9V(A g^{-1})
CDC1/Pd_Cit	0.206	0.834	-61	0.684	341
CDC2/Pd_Cit	0.307	0.844	-66	0.624	289
CDC3/Pd_Cit	0.392	0.858	-61	0.584	414
CDC2/Pd_EG	0.252	0.830	-60	0.512	276
CDC3/Pd_EG	0.356	0.842	-69	0.490	411
C/Pd_Comm	0.589	0.874	-60	0.487	670

In **Table 3**, E1/2 of CDC3/Pd is greater than CDC2/Pd and CDC1/Pd, and thus the activity of ORR for CDC3/Pd is the highest. The low E1/2 and low ORR activity of CDC1/Pd_Cit result from the accumulation of Pd NPs and formation of large Pd NPs in the micropores other than the loading of small particles on the mesopores of the CDC2/Pd_Cit and CDC3/Pd_Cit supports. However, the SA of CDC1/Pd_Cit is higher than the other 2 catalysts, which is also because the Pd NPs are deposited on the mesoporous CDC1, causing the agglomeration of the small NPs and forming large Pd crystallites. Furthermore, with nitrogen doping, the performance of NPs will be improved, and the electro-catalytic activity will be better in comparison to the non-doped NPs as some research claims that the nitrogen doping will raise the number of anchoring sites [10]. The nitrogen doping almost has no effects on the performance and structure of CDC2/Pd_EG and CDC3/Pd_EG catalysts but will decrease the size of the CDC/Pd_Cit. In Table 3, the data shows that the size of the catalysts CDC2/Pd_Cit, and CDC3/Pd_Cit are smaller than the size of catalysts CDC2/Pd_EG and CDC3/Pd_EG respectively. However, the MA of all CDC/Pd_Cit catalysts is higher than all CDC/Pd_EG. Therefore, the size of the Pd NPs is inversely proportional to the MA [9].

4.3. Pd NPs supported on nitrogen-doped graphene quantum dot (NGQD)

PdNGQD-1, PdNGQD-4, PdNGQD-8, and PdNGQD-12 nanocomposites all show electrocatalytic activity for ORR [10]. The ECSA value for PdNGQD-4 is the lowest and for PdNGQD-1 is the highest [11]. Meanwhile, the MA of PdNGQD-1 is the highest and that of PdNGQD-4 is the lowest too, because of the good dispersion and consistent distribution of Pd NPs [10].

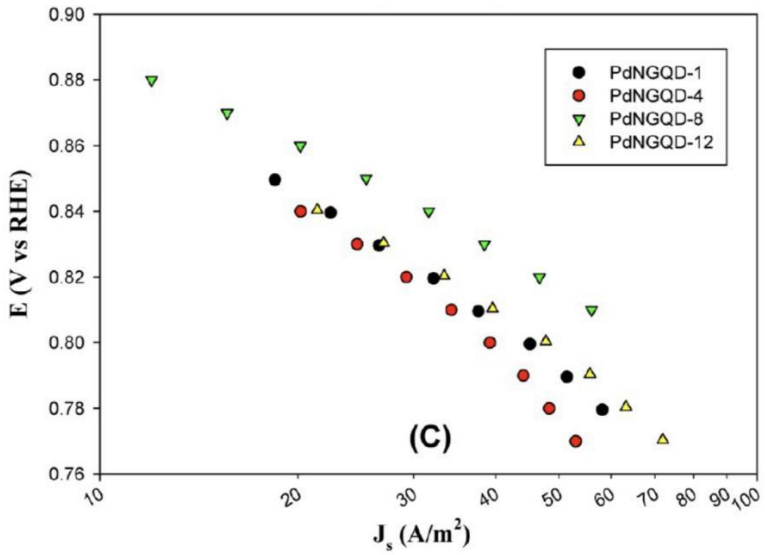

Figure 12. Tafel plots of PdNGQD [10].

The Tafel slope value for PdNGQD-8 is the lowest compared with PdNGQD-1, PdNGQD-4, and PdNGQD-12(**Figure 8**). As lower Tafel slope values and better catalytic performance towards ORR, PdNGQD-8 is considered to be the best catalyst for ORR. In addition, the PdNGQD-8 sample showed the highest SA. [10].

5. Application of Pd/TiO2 decorated carbon fibers for methanol oxidation

Through mapping diagram images, the Pd has been impregnated and located on the surface of the CNTs. There is a positive relationship between EASA and the efficiency of methanol oxidation [2].

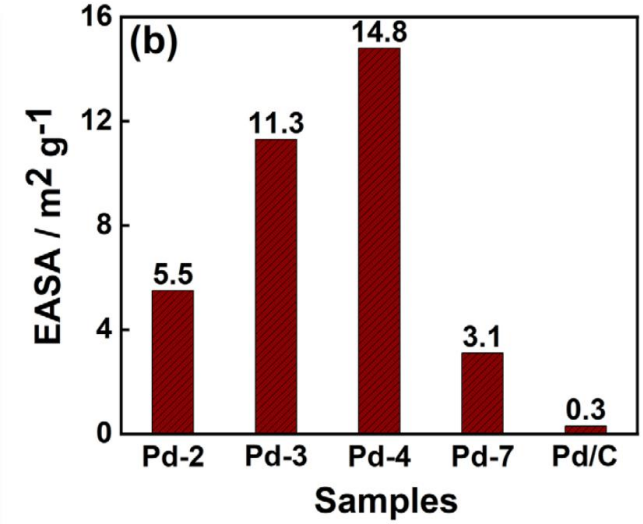

Figure 13. The EASA of Pd/C and Pd@CNTs in KOH [2].

Figure 13 indicates that when the amount of Pd increases, the value of EASA increases and then decreases. The EASA value is the highest when the sample Pd-4 is tested. The rise in the EASA value is mainly because of the incline in Pd loading and more active sites are exposed by Pd, leading to a faster oxidation rate of methanol. The carbon fibers have a sufficiently large exposure area and stronger synergy with Pd, leading to an increase in the catalytic activity. However, as the content of Pd continues increasing, the value of EASA decreases. This is because excessive Pd will result in the accumulation of the Pd NPs and reduce the consistent distribution of the Pd NPs, leading to a large fall of EASA value [2].

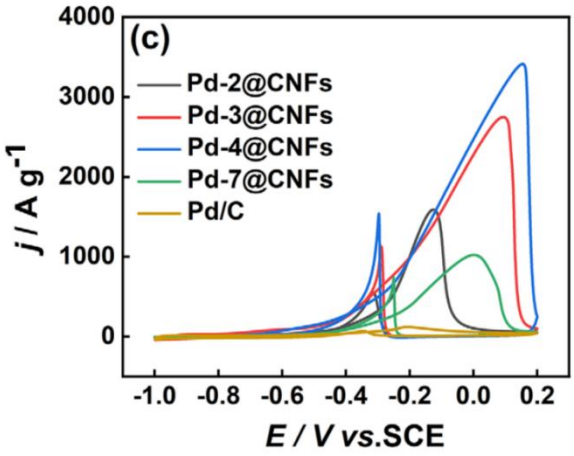

Figure 14. The CVs of Pd@CNFs and Pd/C [2].

The jp value is the anodic peak current density, which represents the catalytic activity of the Pd catalyst. In Figure 14, the jp value of Pd/C is the lowest compared with other Pd@CNFs. The higher jp value of Pd@CNFs than Pd/C when the same amount of Pd is used is attributed to the carbon nanofibers with a greater exposure surface area and more Pd particles exposed, leading to a increase in the contact interface area between the electrolyte and catalyst. Thus, MOR is faster when Pd@CNFs are used, and the electro-catalytic activity is higher [2].

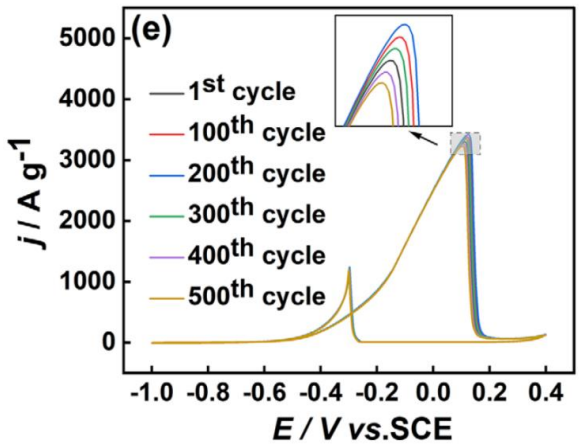

Figure 15. The CVs of the Pd-4@CNFs catalyst for 500 cycles [2].

Moreover, the stability of Pd@CNFs is better than Pd/C when the amount of Pd is the same, and the best electro-catalytic stability is shown by the Pd-4@CNFs. In Figure 15, it is indicated that value of j increases in the first 200 cycles and then decreases after that. Overall, the value of jp only declines 5%, which shows the stability of Pd-4@CNFs [2].

When TiO_2 is added to the Pd-4@CNFs, it will be loaded on the surface of the catalyst. When different amount of the TiO_2 is loaded into the Pd-4@CNFs, there will be different effects on the conductivity, EASA value, and electrochemical activity. The electrical conductivity will be weakened, and the electro-chemical activity of the Pd/TiO_2@CNFs catalyst decreases due to the semi conductivity of TiO_2. However, the synergistic effect between TiO_2 and Pd will enhance the catalytic activity. These two conditions compete and affect the overall electro-catalytic activity of the catalyst. When 5% mass fraction of TiO_2 is added, the electrochemical activity of catalyst is higher compared to the catalyst without TiO_2, and this is due to better synergism between TiO_2 and Pd. When 10% TiO_2 is added, the electrochemical activity of the Pd-4/TiO_2@CNFs catalyst continues to be improved and the EASA value of the Pd-4/TiO_2@CNFs catalyst is maximum. During the methanol oxidation reaction process, the active center of Pd will absorb CO-like intermediates, which will reduce the catalytic activity. The presence of TiO_2 makes itself interact strongly with Pd and reduces the bond

energy between Pd catalysts and the CO-like intermediates. Also, TiO_2 increase the oxidation rate of carbon monoxide by providing the OH- group which is formed from the hydrolysis of water. Thus, the CO-intermediates can quickly leave the active site of Pd and the catalytic activity increases. Meanwhile, if the amount of TiO_2 NPs is in excess, the catalyst conductivity will fall and the TiO_2 also covers the active Pd, leading to a decrease in catalytic performance. Also, occurrence of TiO_2 NPs will negatively affect the stability of the Pd-4-TiO_2@CNFs as the TiO_2 nanoparticles do not bind with Pd and carbon nanofibers ideally [2].

6. Conclusion

In this review, the application of the Pd-based nanomaterials for the ORR that is carried out on the cathode and the MOR that is carried out on the anode are discussed in the direct methanol fuel cells. At first, the mechanisms of ORR and MOR are described. Then, the bimetallic and multi-metallic nanomaterials including Au/C-Pd/C, Pd3Sn/CNTs NHs, and Pd3Ag1/meso-CeO_2 are summarized focusing on stability, the catalytic activity and performance for ORR. Furthermore, supports like rGO with modified POM, CDC, and NGQD that Pd NPs are deposited on will influence the activity of the catalysts for ORR. The study for the use of Pd/TiO_2 decorated carbon fibers for methanol oxidation are also discussed and the effects of different TiO_2 mass fractions on conductivity, EASA value and electrochemical activity will be summarized.

Acknowledgments

The author wishes to acknowledge assistance from Dr Xin Guo of Wenzhou Medical University.

Rerferences

[1] Halim E M, Chemchoub S, El Attar A, Salih F E, Oularbi L, El Rhazi M 2022 *Frontiers* in *Energy Research* **10** 843736

[2] Yin L, Wang C, Liu, Y, Su X, Song Y, Liu Y 2024 *Fuel Cells* e2300113.

[3] Sanij F D, Balakrishnan P, Leung P, Shah A, Su H, Xu Q 2021*International Journal of Hydrogen Energy* 46 14596-14627

[4] Berretti E, Osmieri L, Baglio V, Miller H A, Filippi J, Vizza F, Lavacchi A 2023 *Electrochemical Energy Reviews* **6** 30

[5] Daniel I T, Zhao L, Bethell D, Douthwaite M, Pattisson S, Lewis R J, Hutchings G J 2023 *Catalysis Science & Technology* **13** 47-55

[6] Guo W, Yang R, Fan J, Xiang X, Du X, Shi N, Han M 2024 *RSC advances* **14** 771-778

[7] Sridharan M, Maiyalagan T 2021 *New Journal of Chemistry* **45** 22181-22192

[8] Sanij F D, Balakrishnan P, Su H, Khotseng L, Xu Q 2021 *RSC advances* **11** 39118-39129

[9] Lüsi M, Erikson H, Käärik M, Piirsoo H M, Aruväli J, Kikas A, Tammeveski K 2024 *Nanomaterials* **14** 994

[10] Ejaz A.，Jeon S 2018 *Int. J. Hydrogen Energy* **43** 5690–5702

[11] Deming C P, Mercado R, Lu J E, Gadiraju V, Khan M, Chen S 2016 *ACS Sustainable Chemistry & Engineering* **4** 6580-6589